BIOCHEMISTRY
including biophysical chemistry & molecular biology
Article

Biochemistry **2010,** *49,* 1943–1953 1943
DOI: 10.1021/bi901730x

Biochemical and Structural Properties of Chimeras Constructed by Exchange of Cofactor-Binding Domains in Alcohol Dehydrogenases from Thermophilic and Mesophilic Microorganisms‡

Edi Goihberg,§ Moshe Peretz,§ Shoshana Tel-Or,§ Orly Dym,∥ Linda Shimon,⊥ Felix Frolow,@ and Yigal Burstein*,§

§*Department of Organic Chemistry,* ∥*Department of Structural Biology and Israel Structural Proteomics Center, and* ⊥*Department of Chemical Research Support, Weizmann Institute of Science, Rehovot 76100, Israel, and* @*Department of Molecular Microbiology and Biotechnology, The George S. Wise Faculty of Life Sciences and the Daniella Rich Institute for Structural Biology, Tel-Aviv University, Ramat Aviv 69978, Israel*

Received October 7, 2009; Revised Manuscript Received December 31, 2009

ABSTRACT: The cofactor-binding domains (residues 153−295) of the alcohol dehydrogenases from the thermophile *Thermoanaerobacter brockii* (TbADH), the mesophilic bacterium *Clostridium beijerinckii* (CbADH), and the protozoan parasite *Entamoeba histolytica* (EhADH1) have been exchanged. Three chimeras have been constructed. In the first chimera, the cofactor-binding domain of thermophilic TbADH was replaced with the cofactor-binding domain of its mesophilic counterpart CbADH [chimera $X21_{(TCT)}$]. This domain exchange significantly destabilized the parent thermophilic enzyme ($\Delta T_{1/2} = -18$ °C). The reverse exchange in CbADH [chimera $X22_{(CTC)}$], however, had little effect on the thermal stability of the parent mesophilic protein. Furthermore, substituting the cofactor-binding domain of TbADH with the homologous domain of EhADH1 [chimera $X23_{(TET)}$] substantially reduced the thermal stability of the thermophilic ADH ($\Delta T_{1/2} = -51$ °C) and impeded the oligomerization of the enzyme. All three chimeric proteins and one of their site-directed mutants were crystallized, and their three-dimensional (3D) structures were determined. Comparison of the 3D structures of the chimeras and the chimeric mutant with the structures of their parent ADHs showed no significant changes to their Cα chains, suggesting that the difference in the thermal stability of the three parent ADHs and their chimeric mutants could be due to a limited number of substitutions located at strategic positions, mainly at the oligomerization interfaces. Indeed, stabilization of the chimeras was achieved, to a significant extent, either by introduction of a proline residue at a strategic position in the major horse liver ADH-type dimerization interface ($\Delta T_{1/2} = 35$ °C) or by introduction of intersubunit electrostatic interactions ($\Delta T_{1/2} = 6$ °C).

The dependence of the quantitative effects evoked by a given mutation on the framework in which it is introduced has gradually become recognized. Such mutations can be studied using chimeric enzymes, genetically engineered hybrid proteins made by splicing genes from two or more different enzymes. For example, Loung and Kirsch (*1*) proposed that the contribution of a X → Y mutation to thermostability might depend on whether a neighboring residue is W or Z, in other words, on the context of the background in which the mutation is introduced. When the two sites of substitution are well separated, the cumulative effect of mutations is usually additive, but less so when they are spatially adjacent (*2*). In this sense, working with chimeric enzymes is an advantage because interchanging entire fragment(s) comprising certain structural feature(s) or domain(s) between thermophilic and mesophilic enzymes preserves the structural environment of that structural feature(s) or domain(s). Thus, the ability to probe the contribution of a certain structural feature or domain to the thermostability of the thermophilic protein also provides a potent tool for selecting significant region(s) from several different candidates. The members of an enzyme family used for the construction of chimeric enzymes should have not only a high degree of amino acid sequence identity but also similar three-dimensional (3D) structures. In such cases, the inserted fragment(s) fits into a similar environment and thus would not perturb the proximal and overall structure of the accepting enzyme. Hence, any change in thermostability following an interchange(s) of fragment(s) or domain(s) would be attributable to such interchange(s). When a chimera is constructed via replacement of nonhomologous fragments, changes in the overall 3D structure of the chimeric enzyme are introduced; hence, no specific contribution of the new inserted structural element can be deduced.

Several investigators have examined the thermostability of chimeric enzymes using different systems. For example, the Arnold group applied the structural computational approach SCHEMA, for probing the stability of chimeras of homologous proteins (*3*). They showed that predicted sequence blocks make additive contributions to the thermal stability of chimeras of cytochrome P450. The same group, using the same approach, engineered chimeras of CBH II cellulases, with enhanced thermal stability (*4*). Bergeron et al. demonstrated yet another interesting approach to stabilization of proteins via chimerization where penicillin amidase and a thermophilic chaperonin were fused to

‡The Protein Data Bank entries are 3FPC for chimera $X23_{(TET)}$, 3FPL for chimera $X22_{(CTC)}$, 3FSR for chimera $X21_{(TCT)}$, and 3FTN for double mutant chimera Q165E/S254K-$X21_{(TCT)}$.

*To whom correspondence should be addressed: Department of Organic Chemistry, Weizmann Institute of Science, Rehovot 76100, Israel. Phone: +972-8-9343828. Fax: +972-8-9342501. E-mail: yigal.burstein@weizmann.ac.il.

Published on Web 01/26/2010

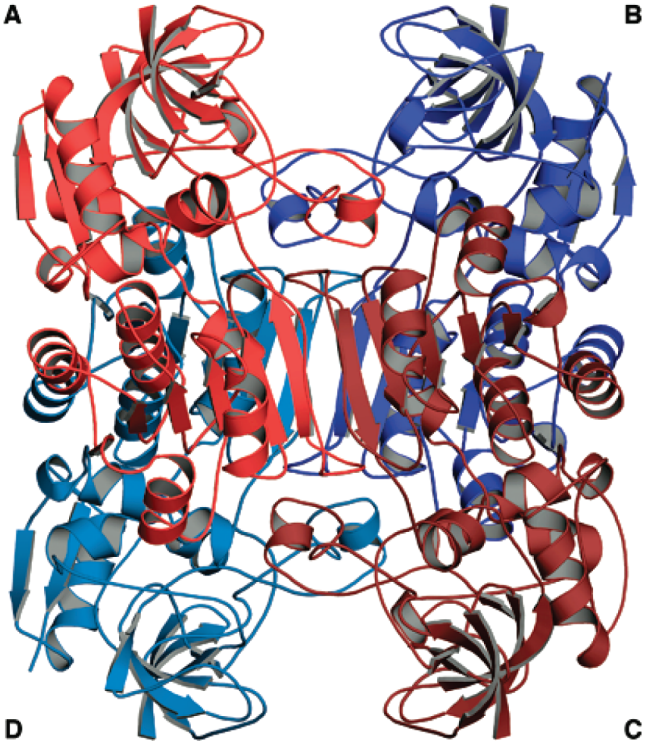

FIGURE 1: Cartoon representation of tetrameric TbADH. Monomeric subunits A−D are annotated and colored in different colors. The horse liver alcohol dehydrogenase type dimers are the AC and BD pairs.

produce a chimera with increased thermostable activity of amoxicillin synthesis (*5*).

Among the various dehydrogenases studied as model systems for studying thermostability (e.g., refs *6*−*10*), the secondary alcohol dehydrogenases (*11*, *12*) are of special biotechnological interest because they are useful chiral synthesizing reagents (*13*, *14*).

Secondary alcohol dehydrogenases have been extensively studied by our group. The $NADP^+$-dependent alcohol dehydrogenases from the thermophile *Thermoanaerobacter brockii* (TbADH),[1] the mesophilic bacterium *Clostridium beijerinckii* (CbADH), and the protozoan parasite *Entamoeba histolytica* (EhADH1, EC 1.1.1.2) are homotetrameric, medium chain secondary alcohol dehydrogenases (*15*, *16*). The structures of TbADH, CbADH, and EhADH1 comprise four identical 38−39 kDa polypeptide chains composed of 352, 351, and 360 amino acids, respectively, and contain Zn^{2+} at the active site (see, e.g., Figure 1). The monomer is composed of two discrete domains (*17*, *18*), the cofactor-binding domain [residues 154−294 (Figure 2)] and the catalytic domain [residues 1−153 and 295−351 (Figure 2)]. These are separated by a deep cleft. All three enzymes use $NADP^+$(H) as a coenzyme and a secondary alcohol as the substrate (*15*, *16*). Amino acid sequence alignments of the three ADHs revealed a high degree of sequence conservation among the three members of this enzyme family: 75% identity between TbADH and CbADH, 66% identity between EhADH1 and TbADH, and 62% identity between EhADH1 and CbADH (*15*, *16*).

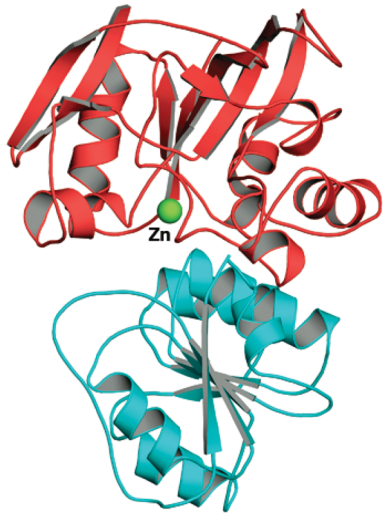

FIGURE 2: Ribbon representation of the monomer of chimera $X21_{(TCT)}$. The cofactor-binding domain (residues 154−294) and the catalytic domain (residues 1−153 and 295−351) are colored cyan and red, respectively. The catalytic zinc ion is shown as a sphere.

Despite their high degree of sequence homology, the enzymes differ greatly in thermostability. We determined that the thermophile TbADH reversibly catalyzes the oxidation of secondary alcohols to the corresponding ketones with a $T_{1/2}^{60\ min}$ (the temperature at which 50% of the enzymatic activity is lost after incubation for 1 h, interpolated from a plot of the residual enzymatic activity vs temperature) of >90 °C. Although the hosts of CbADH and EhADH1 grow at ~30−37 °C and are thus considered mesophiles, their ADHs are thermostable: $T_{1/2}^{60\ min}$ for CbADH of 66.5 °C and $T_{1/2}^{60\ min}$ for EhADH1 of 77.5 °C. The stability of their secondary structures also differs, as judged by circular dichroism (CD) studies; the $T_{1/2}^{CD}$ values (thermal denaturation midpoint monitored by the change in CD ellipticity at 218 nm) of TbADH, CbADH, and EhADH1 are 93.8, 67.5, and 80 °C, respectively (*19*).

Previously applying the site-directed mutagenesis (SDM) approach, we have shown that strategic placement of proline residues and intersubunit salt bridges can account for the differences in thermostability between the ADHs (*19*, *20*). A previous study of our group of chimeras between TbADH and CbADH was conducted using random chimerical constructs. The thermal stability of each chimeric enzyme was approximately exponentially proportional to the content of the amino acid sequence of the thermophilic enzyme, indicating that the amino acid residues contributing to the thermal stability of TbADH are distributed along the whole protein molecule (*21*). We were intrigued by the fact that the ADHs monomer are composed of two structurally discrete domains (Figure 2); moreover, most of the intersubunit contacts in the tetramer are located in the cofactor-binding domain and in a protruding lobe in the catalytic domain (*17*, *18*).

In this study, we constructed, cloned, and overexpressed the genes encoding chimeric ADHs composed of switch domains that are derived from TbADH, CbADH, and EhADH1 and purified and characterized the recombinant chimeric ADHs. The chimeras were crystallized, and their 3D structures were determined. On the basis of their structures. SDM was performed upon the chimeric constructs. The mutant chimeras were purified and characterized, and the 3D structure of one chimeric mutant with enhanced thermal stability was determined.

[1]Abbreviations: ADH, alcohol dehydrogenase; CbADH, *C. beijerinckii* ADH; EhADH1, *E. histolytica* ADH; HLADH, horse liver ADH; TbADH, *T. brockii* ADH; ANS, 1-anilino-8-naphthalenesulfonate; CD, circular dichroism; DTT, dithiothreitol; EDTA, ethylenediaminetetraacetic acid; NADP, nicotinamide adenine dinucleotide phosphate; PDB, Protein Data Bank; SDM, site-directed mutagenesis; Rec, recombinant; rmsd, root-mean-square deviation; SDS−PAGE, sodium dodecyl sulfate−polyacrylamide gel electrophoresis; Tris, tris(hydroxymethyl)aminomethane.

MATERIALS AND METHODS

Construction of the Chimeras and Site-Directed Mutagenesis. The enzymes for DNA cloning, sequencing, and amplification were purchased from Amersham, New England Biolabs (Ipswich, MA), Fermentas MBI (Burlington, ON), and Promega (Madison, WI). Oligonucleotides for cloning, sequencing, and site-directed mutagenesis of the *T. brockii, E. histolytica*, and *C. beijerinckii adh* genes were synthesized by the WIS Chemical Synthesis Laboratory. All other chemicals were of analytical grade. The genes encoding TbADH and EhADH1 were constructed and expressed according to the methods of Goihberg et al. (*22*) and Peretz et al. (*16*) using plasmids $pBSP80^{TbADH}$, $pBSP80^{EhADH1}$, and $pBSP80^{CbADH}$ (*23*) as templates for generating the recombinant chimeras and their mutant variants.

The chimeric enzymes were constructed as follows. First, to introduce the restriction sites for AgeI (at position 460) and for BsaI (at position 883) into the TbADH, CbADH, and EhADH1 genes, we incorporated silent mutations, as described below at base pairs 462, 879, and 882 in the TbADH gene, base pairs 462, 465, 882, 885, and 888 in the CbADH gene, and base pairs 462, 465, 880, 882, 883, and 884 (Thr295 to Cys) in the EhADH1 gene. All recombinant plasmids harboring the mutant variants were transformed into *Escherichia coli* strain TG-1. DNA was extracted using a DNA purification kit (Boehringer Mannheim). The DNA was then digested with the restriction enzymes AgeI and BsaI; the digest was subjected to electrophoresis on a 2% agarose gel, and the respective DNA fragments were eluted from the gel using the Boehringer Mannheim kit for PCR product purification. Finally, the DNA fragment (424 bp long, corresponding to base pairs 460−883 of the CbADH gene) was ligated to linearized plasmid $pBS80^{TbADH}$ lacking its original 460−883 bp fragment, producing the $X21_{(TCT)}$ chimera. The 460−883 bp DNA fragment of TbADH was ligated into linearized plasmid $pBS80^{CbADH}$ lacking its original 460−883 bp fragment, producing the $X22_{(CTC)}$ chimera. The 460−883 bp fragment of EhADH1 was ligated into linearized plasmid $pBS80^{TbADH}$ lacking its original 460−883 bp fragment, producing the $X23_{(TET)}$ chimera. The ligation products were transformed into *Es. coli* strain TG-1 and screened as described below.

SDM was performed using the QuikChange XL site-directed mutagenesis kit from Stratagene (La Jolla, CA). The mutations were verified by DNA sequencing of the corresponding plasmids. The forward primers used for generating the mutants are listed below, with the exchanged bases underlined. The sequences of the corresponding reverse primers were complementary to the forward primers: AgeI restriction site in TbADH, 5′-CCCGATATGATGACCGGTTTTCACGGAGCTG-3′; BsaI restriction site in TbADH, 5′-CATAAAACTATAAAAGGCGGTCTCTGCCCCGGTGGACG-3′; AgeI restriction site in CbADH, 5′-GATAACAGATATGACTACCGGTTTTCATGGAGCAGAAC-3′; BsaI restriction site in CbADH, 5′-GACTATAAAAGGTCTCTGCCCCGGGGGACGTTTG-3′; AgeI restriction site in EhADH1, 5′-GATATGGTAACTACCGGTTTCCATGGAGCAGAATTAG-3′; BsaI restriction site in EhADH1, 5′-CTGACTCTTCCACCTGGGCAGAGACCTCCATGAATG-3′; for Q165E-$X21_{(TCT)}$, 5′-GAGCAGAACTTGCAGATATTGAAATGGGTTCAAGTG-3′; for S254K-$X21_{(TCT)}$, 5′-CTGAAACATTATCCCAAGCAGTAAAGATGGTTAAACCAGGAGG-3′; for D275P-$X23_{(TET)}$, 5′-GAGAAGGAGATAATATTCCTATTCCAAGAAGTGAATGGGG-3′.

Expression and Purification of the Recombinant Enzymes. All recombinant plasmids bearing TbADH, EhADH1, and CbADH, their recombinant chimeric constructs, and the chimeric mutant variants were transformed into *Es. coli* strain TG-1, and the recombinant proteins were purified according to a modification of a procedure described by Peretz and Burstein (*11*). Briefly, the transformed cells were cultured for 17 h in 2YT with zinc chloride (50 μM) and ampicillin (100 mg/L) at 37 °C, harvested by centrifugation for 20 min at 8000*g* (4 °C), and resuspended in buffer A [25 mM Tris-HCl (pH 7.3), 0.1 mM DTT, 0.1 mM EDTA, 0.1 mM benzamidine, 0.02% sodium azide, and 10% glycerol]. Cells were disrupted by pulsed sonication for 5 min (Branson Sonifier 450), using a rosette cup immersed in an ice bath, and then centrifuged (100000*g* for 15 min at 4 °C) to remove cell debris. The supernatant was then heat-treated for 3 min at 65 °C [except for the $X23_{(TET)}$ chimera and its D275P-$X23_{(TET)}$ mutant] and recentrifuged for 15 min at 30000*g* (4 °C). The clear supernatant was loaded onto a DEAE-52-cellulose column (10 cm × 3 cm), previously equilibrated with buffer A at 4 °C. The column was extensively washed with buffer A until no protein was detected in the eluted buffer (measured according to the method of Bradford) (*24*). The retained proteins were eluted from the column with buffer A containing 0.1 M NaCl at a rate of 1 mL/min. Fractions containing enzymatic activity were pooled, concentrated by ultrafiltration, dialyzed against buffer A, and then applied onto a short Red Sepharose column (12 cm × 3 cm) (Pharmacia, Uppsala, Sweden). The purified recombinant enzyme was eluted from the Red Sepharose column with a 400 mL linear gradient of NaCl from 0.1 to 1 M for TbADH, from 0.1 to 2 M for CbADH, and from 50 to 250 mM for EhADH1 in buffer A at a flow rate of 1 mL/min. Fractions containing ADH enzymatic activity were collected, concentrated by ultrafiltration (Amicon YM-30), and stored in 50% glycerol at −20 °C. The purity of the enzymes was determined by Coomassie Brilliant Blue staining of SDS−12% polyacrylamide gel electrophoresis (PAGE) gels.

Enzyme Assay. The catalytic activity of the ADHs at 40 °C was measured by following the reduction of $NADP^+$ and monitoring the formation of NADPH, at 340 nm (ε_{340} = 6.2 mM^{-1} cm^{-1}). The standard assay mixture contained 150 mM 2-butanol, 0.5 mM $NADP^+$, and 100 mM Tris-HCl (pH 9.0) in a total volume of 1 mL. One unit of ADH activity is defined as the amount of enzyme that catalyzes the oxidation of 1 μmol of 2-butanol/min at 40 °C at the initial velocity under the conditions described above. Kinetic parameters were measured and calculated using a Beckman DU-7500 spectrophotometer equipped with a Multicomponent/SCA/Kinetics Plus software package and a Peltier temperature controller. The kinetic parameters for 2-butanol were determined using increasing concentrations of the alcohol (0.1−100 mM) and enzyme (5−120 nM) with 0.5 mM $NADP^+$ in 100 mM Tris-HCl (pH 9.0). The value presented is the mean of three experiments; individual measurements were within 10% of the quoted mean.

Circular Dichroism Measurements. Far-UV (200−260 nm) CD spectra were recorded over a temperature range of 30−98 °C with an average increase in temperature of 1 °C/min, using an Aviv model 202 CD spectrophotometer. Scans were performed every 4 °C using 13 μM (0.5 mg/mL) protein in 50 mM Na/K phosphate buffer (pH 6.8), in quartz cells with a light path of 0.1 cm. Data (millidegrees vs wavelength) were collected every nanometer with an averaging time of 2 s. The background CD signal for each analysis, determined in a single scan using buffer

alone at 25 °C, was subtracted from each scan and was temperature-independent. The decrease in the magnitude of the CD signal with the increase of temperature was evaluated at the local minima of 218 nm and further normalized by subtracting from each wavelength the lowest signal observed at that particular wavelength. The change in the percent residual CD signal was plotted as a function of temperature, and the residual 50% CD signal ($T_{1/2}^{CD}$) was estimated.

Thermal Inactivation ($T_{1/2}^{60\ min}$ *and* $T_{1/2}^{CD}$). The thermal stability of the ADHs was determined by monitoring the residual enzymatic activity after incubation for 60 min in 50 mM Na/K phosphate buffer and 1 M NaCl (pH 6.8) at different temperatures. $T_{1/2}^{60\ min}$ is the temperature at which 50% of the enzymatic activity is lost after incubation for 1 h, interpolated from a plot of the residual enzymatic activity versus temperature. $T_{1/2}^{CD}$ is the temperature at which 50% of the original CD signal at 218 nm is lost upon heating the protein sample between 30 and 98 °C, with an average increase in temperature of 1 °C/min. The value presented is the mean of three experiments; individual measurements were within 2.5% of the quoted mean.

Fluorescence Measurements. Fluorescence measurements were performed on a JASCO 8100 fluorometer. Solutions contained the protein at a concentration of 0.1 mg/mL in 50 mM Na/K phosphate buffer (pH 6.8), previously incubated for 1 h with a 50-fold molar excess of 1-anilino-8-naphthalenesulfonate (ANS). The excitation was set at 380 nm, and the emission wavelength ranged from 400 to 630 nm. Each plot is an average of three experiments.

Analytical Procedures. DNA sequencing was performed with an Applied Biosystems model 373A DNA sequencer using the dideoxy method of Sanger and Coulson (*25*) and appropriate primers. SDS−PAGE was performed on 12% slab gels and 5% stacking gels according to the method of Laemmli (*26*) (Bio-Rad MiniProtean II system) and stained with Coomassie Brilliant Blue. Protein concentrations were determined according to method of Bradford (*24*), using bovine serum albumin as the standard. Size exclusion experiments were performed on a Superdex 200HR 10/30 column with an AKTA Purifier FPLC (Amersham Pharmacia Biotech).

Crystallization, Diffraction Experiments, Structure Determination, and Data Refinement. (*i*) *X23*$_{(TET)}$. Single crystals of apo-X23$_{(TET)}$ were obtained by the vapor diffusion method at 18 °C, when 1 μL of apo-X23$_{(TET)}$ stock solution [8 mg/mL protein, 25 mM Tris-HCl, 50 mM NaCl, 0.1 mM DTT, and 50 mM $ZnCl_2$ (pH 7.5)] was mixed with 1 μL of reservoir solution [16% (w/v) PEG 8K, 200 mM magnesium acetate tetrahydrate, and 100 mM cacodylate buffer (pH 6.5)].

(*ii*) *X21*$_{(TCT)}$. Single crystals of apo-X21$_{(TCT)}$ were obtained by the microbatch method under oil at 18 °C, using the IMPAX 1-5 robot (Douglas Instruments Ltd.). X21$_{(TCT)}$ (6 mg/mL) was crystallized in a mixture containing 50 mM acetate, 400 mM NaH_2PO_4/600 mM K_2HPO_4 (pH 6.7), 12.5 mM Tris-HCl (pH 7.5), 25 mM NaCl, 50 μM DTT, and 25 μM $ZnCl_2$.

(*iii*) *X22*$_{(CTC)}$. Single crystals of apo-X22$_{(CTC)}$ were obtained by the microbatch method under oil at 18 °C, using the IMPAX 1-5 robot. The apo-X22$_{(CTC)}$ (10 mg/mL) was crystallized in a mixture containing 100 mM ammonium acetate, 15% (w/v) PEG 4K, 25 mM NaCl, 50 μM DTT, 25 μM $ZnCl_2$, and 50 mM tricitrate dihydrate (pH sodium 5.6).

(*iv*) *Q165E*/*S254K*-*X21*$_{(TCT)}$. Single crystals of apo-Q165E/S254K-X21$_{(TCT)}$ were obtained by the microbatch method under oil at 18 °C, using the IMPAX 1-5 robot. The protein (10 mg/mL) was crystallized in a mixture containing 5% (w/v) PEG 800, 25 mM NaCl, 50 μM DTT, 25 μM $ZnCl_2$, 50 μM imidazole (pH 8), and 12.5 mM Tris-HCl (pH 7.5).

Diffraction Data Collection. Crystals of X23$_{(TET)}$ and X22$_{(CTC)}$ were delivered to the synchrotron (ESRF) packed with mother liquor in glass capillaries sealed by fire. Prior to data collection under cryogenic conditions, crystals were transferred to a cryo-solution for a period of 10 min before being mounted in a rayon fiber loop (*27*) and flash-cooled in the flow of cold nitrogen at 100 K. Data sets from X23$_{(TET)}$ and X22$_{(CTC)}$ crystals were collected to 1.40 and 1.90 Å resolution, respectively, as 0.5° oscillation frames, 5 s/frame, at a distance of 120 mm with an ADSC CCD detector at beamline ID14-2 at ESRF (λ = 0.933 Å).

Data sets from X21$_{(TCT)}$ and Q165E/S254K-X21$_{(TCT)}$ were collected to 2.2 Å resolution using in-house X-ray facilities equipped with a Rigaku RU-3HR 18KW-rotating anode, a RAXIS-IV^{++} imaging plate detector, Osmic multilayer focusing mirrors, and low-temperature Oxford Cryostream systems.

The diffraction data were processed with DENZO and SCALEPACK incorporated into HKL2000 (*28*). The crystal and data parameters are summarized in Results.

Structure Determination. All structures were determined by molecular replacement (MOLREP) (*29*) using the monomer of TbADH (PDB entry 1YKF) as a search model, using a resolution range of 40.0−2.5 Å. The cross-rotation function in each case revealed a group of major peaks (measured in standard deviation or σ units) related to the correct solutions with a large gap to the next peaks (data not shown). The translation search gave a clear solution in each case.

Structure Refinement. After molecular replacement, 20 cycles of the rigid body and 10 cycles of the restrained refinement were executed using REFMAC5 (*30*) as implemented in CCP4 (*31*) with CCP4i GUI (*32*). A random set consisting of 5% of the reflections was excluded from calculations for cross validation of various refinement strategies (*33*) such as geometric and temperature factor restraints (reassessed at various stages of refinement), for solute molecule insertion, and for a basis for the maximum-likelihood refinement protocol implemented in REFMAC5 (*30*). To estimate the potential limit of the model convergence and to eliminate model bias, ARP/WARP 6.0 and later ARP/WARP 7.0 for improvement and objective interpretation of crystallographic electron density maps and automatic construction and refinement of macromolecular models were implemented using the mode of map improvement by atoms update and refinement (*34*). The resulting temporary coordinate files were hybrids in a sense that in addition to atoms of the protein molecule they contained dummy atoms that modeled features of the electron density map dissimilar to the model or missing from the model: water and other solute molecules and alternative conformations. This hybrid coordinate file was input to 10 cycles of REFMAC5 refinement. The electron density maps were calculated with likelihood-weighted $2|F_o| - |F_c|$ and $|F_o| - |F_c|$ coefficients, and the protein structure was reinterpreted using COOT (*35*).

The catalytic Zn ions were unambiguously detected in the active sites of the ADH structures by inspection of likelihood-weighted $2|F_o| - |F_c|$ and $|F_o| - |F_{calc}|$ and Δ_{anom} electron density maps. After structure reinterpretation, the dummy atoms were deleted from the coordinate list and the improved model gradually emerged during cycles of rebuilding and refinement. Clear electron density representing alternative conformations was observed near several amino acid chains, which were

subsequently modeled as alternative, mutually exclusive conformations. Water molecules were assigned initially automatically using COOT (*35*). At the later stage of water insertion, difference electron density map peaks were inspected manually and the decision to insert them was based on the electron density peak's appearance, value, location, and distance from the nearby structural elements. The occupancy factors of solvent molecules were assumed to be unity, except for water molecules associated with the alternative side chain conformations, where they were set according to alternative side chain occupancies. Scaling parameters, bulk solvent correction, atomic coordinates, TLS parameters (*36*), isotropic thermal parameters for $X21_{(TCT)}$, $X22_{(CTC)}$, and Q165E/S254K-$X21_{(TCT)}$, and anisotropic thermal parameters for $X23_{(TET)}$ were refined during the last cycles of refinement. Quality assessment was done using PROCHECK (*37*), WHATIF (*38*), MOLPROBITY (*39*), and COOT (*35*). Refinement parameters are summarized in Results. Additional refinement information is contained in PDB entries 3FPC for chimera $X23_{(TET)}$, 3FPL for chimera $X22_{(CTC)}$, 3FSR for chimera $X21_{(TCT)}$, and 3FTN for double mutant chimera Q165E/S254K-$X21_{(TCT)}$.

RESULTS

Constructs of the Chimeras. Recombinant chimeric ADHs containing different segments of TbADH, CbADH, and EhADH1 were constructed, overexpressed, purified, and characterized. The first chimera, denoted $X21_{(TCT)}$, comprises the catalytic domain of TbADH (residues 1−152 and 296−352) and the cofactor-binding domain of CbADH (residues 153−295). Another chimera, denoted $X22_{(CTC)}$, comprises the catalytic domain of CbADH (residues 1−152 and 296−351) and the cofactor-binding domain of TbADH (residues 153−295). A third chimera, denoted $X23_{(TET)}$, comprises the catalytic domain of TbADH (residues 1−152 and 296−352) and the cofactor-binding domain of EhADH1 (residues 153−295).

The purified recombinant chimeras were characterized by SDS−PAGE, displaying apparent molecular masses of 38 kDa per monomer, similar to those of the wild-type enzymes (data not shown).

Quaternary Structure of the Chimeric ADHs. The purified chimeric enzymes were subjected to gel filtration chromatography on a Superdex 200 column. The results presented in Figure 3 show that $X21_{(TCT)}$ and $X22_{(CTC)}$ eluted as tetramers with retention times identical to those of their parent proteins, whereas $X23_{(TET)}$ eluted predominantly as a monomer.

Enzymatic Properties of the Chimeras. Table 1 shows that the enzymatic properties of chimeras $X21_{(TCT)}$ and $X22_{(CTC)}$ were rather similar to those of their parent enzymes. On the other hand, the specific activity of the $X23_{(TET)}$ chimera was only < 2% of that of the parent enzymes, implying that the monomer of the $X23_{(TET)}$ chimera is enzymatically inactive. The traces of enzymatic activity of the $X23_{(TET)}$ chimera could be assigned to traces of the tetrameric species of that chimera.

Circular Dichroism Studies of $X23_{(TET)}$. We probed the secondary structure of monomeric chimera $X23_{(TET)}$ (protein peak eluted at 15 mL in Figure 3) by far CD spectroscopy. As shown in Figure 4, the far CD spectrum profile of $X23_{(TET)}$ is almost identical to those of its parent ADHs EhADH1 and TbADH, implying that upon dissociation to monomers, $X23_{(TET)}$ retains the gross elements of secondary structure of the tetramer components.

1-Anilino-8-naphthalenesulfonate Binding Studies of $X23_{(TET)}$. Binding of ANS to the hydrophobic regions of proteins results in an increase in the fluorescence intensity and can be indirectly referred to the conformational rigidity of the protein (*40*). Therefore, we tested the exposure of the hydrophobic surface of $X23_{(TET)}$ to the solvent by its capacity to bind ANS. Figure 5 shows the fluorescence spectra of ANS bound to EhADH1, TbADH, and $X23_{(TET)}$ in the range of 400−650 nm, at a protein concentration of 2.5 μM (0.1 mg/mL). The results show that the fluorescence intensity of ANS bound to $X23_{(TET)}$ (monomer) is 50% higher than that of ANS bound to TbADH and EhADH1 (tetramers). This result indicates that the hydrophobic regions of the ADHs that are involved in maintaining the quaternary structure of the tetramer and intramolecular interfaces (e.g., between the catalytic and coenzyme-binding domains) have been at least partially exposed upon dissociation to monomers in $X23_{(TET)}$.

Thermal Stability Parameters of the Chimeric ADHs. The thermal stability parameters of the chimeras are presented in Table 2. The changes in the CD signals of the ADHs as a function of temperature are presented in Figure 6. The narrow CD signal drop as a function of temperature of $X23_{(TET)}$ indicates that the monomeric state has a well-defined structure as opposed to an unstructured state like a molten globule. The finding that the

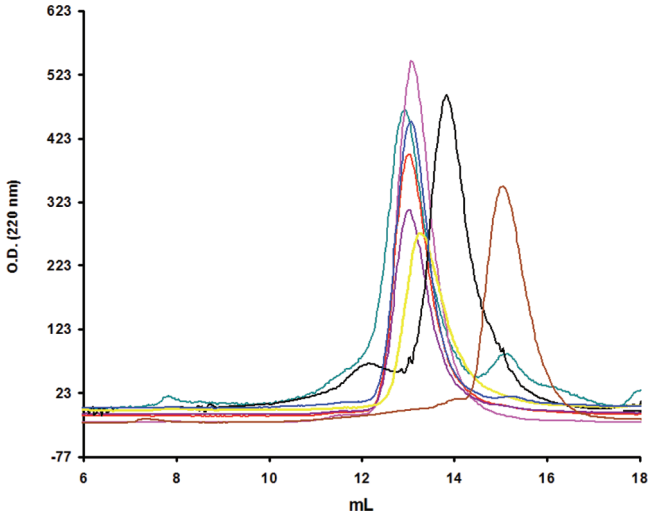

FIGURE 3: Size exclusion chromatograms of chimeric ADHs. The ADHs and their chimeras were loaded onto a Superdex HR200 10/30 column (Pharmacia). The column was eluted with 100 mM NaCl and 50 mM Tris-HCl (pH 7.5) at a flow rate of 0.5 mL/min: $X21_{(TCT)}$, yellow; $X22_{(CTC)}$, blue; $X23_{(TET)}$, brown; D275P-$X23_{(TET)}$, green; Rec-CbADH, red; Rec-EhADH1, violet. Rec-TbADH (cyan) and commercial HLADH (horse liver ADH, black), serve as tetramer and dimer markers, respectively.

Table 1: Kinetic Parameters of the ADHs[a]

ADH	K_m (mM)	k_{cat} (min^{-1})	k_{cat}/K_m (mM^{-1} min^{-1})
TbADH	3.1	1724	556
$X21_{(TCT)}$	2.1	2689	1280
CbADH	13.0	9714	747
$X22_{(CTC)}$	9.8	3565	364
EhADH1	0.74	3025	4088
$X23_{(TET)}$	ND[b]	ND[b]	

[a]Enzymatic activity was measured by monitoring the formation of NADPH at 340 nm. K_m values for 2-butanol were determined with varying concentrations of 2-butanol (0.1−100 mM), enzyme (5−120 nM), and 0.5 mM $NADP^+$ in 100 mM Tris-HCl (pH 9) in a total volume of 1 mL, in triplicates. Values are averages of two experiments, and the individual measurements were within 10% of the quoted mean. [b]Nondetectable.

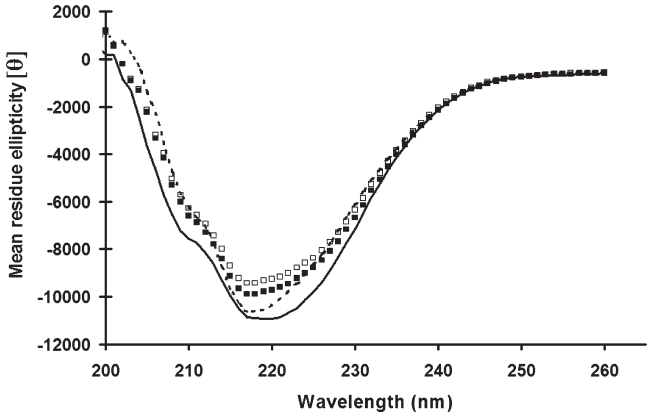

FIGURE 4: Far-UV CD spectra of TbADH, EhADH1, and $X23_{(TET)}$. The data (mean residual ellipticity vs wavelength) were collected every nanometer with an averaging time of 2 s using quartz cells with a light path of 0.1 cm. The protein concentration was ca. 0.5 mg/mL in 50 mM Na/K phosphate buffer (pH 6.8). Each plot is an average of three experiments: TbADH (---), EhADH1 (—), chimera $X23_{(TET)}$ (□), and chimeric mutant D275P-X23 (■).

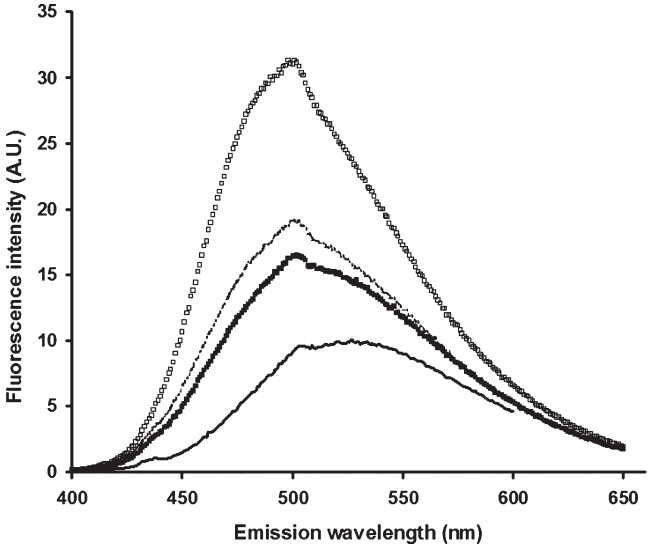

FIGURE 5: Fluorescence emission spectra of ANS bound to TbADH, EhADH1, and $X23_{(TET)}$. The excitation wavelength was 380 nm, and the emission wavelength ranged from 400 to 630 nm. The sample contained the protein at a concentration of 0.1 mg/mL in 50 mM Na/K phosphate buffer (pH 6.8), previously incubated with a 50-fold molar excess of ANS. Each plot is an average of three experiments: ANS (—), TbADH (■), EhADH1 (---), and chimera $X23_{(TET)}$ (□).

$T_{1/2}{}^{CD}$ value of monomeric chimera $X23_{(TET)}$ is 39 and 25 °C lower than the $T_{1/2}{}^{CD}$ values of its respective tetrameric "parent" enzymes, TbADH and EhADH1, respectively (Table 2), indicates the contribution of the intersubunit interactions to the thermostability of the native tetrameric enzymes. Likewise, the significant reduction in the $T_{1/2}{}^{60\ min}$ value of tetrameric chimera $X23_{(TET)}$, which is 50.8 and 34.5 °C lower than the $T_{1/2}{}^{60\ min}$ values of TbADH and EhADH1, respectively, indicates that the chimera lacks crucial stabilizing elements that maintain the integrity of the tetrameric state of the parent enzymes.

3D Structures of Chimeric ADHs. The structures of $X21_{(TCT)}$, $X22_{(CTC)}$, and $X23_{(TET)}$ chimeras were determined by X-ray crystallography to 2.2, 1.9, and 1.4 Å resolution, respectively. Data collection and refinement statistics are listed in Table 3.

All chimeras, including $X23_{(TET)}$ (most of which was present in solution as monomer), crystallized in their tetrameric form.

Table 2: Thermal Parameters of Native and Chimeric ADHs and Their Mutants

	$T_{1/2}{}^{60\ min}$ (°C)[a]	$\Delta T_{1/2}{}^{60\ min}$ (°C)	$T_{1/2}{}^{CD}$ (°C)[b]	$\Delta T_{1/2}{}^{CD}$ (°C)
TbADH	93.8		93.8	
CbADH	66.5		67.5	
EhADH1	77.5		80	
$X21_{(TCT)}$	72	−21.8[c]	76	−17.8[c]
$X22_{(CTC)}$	66	−0.5[d]	70	2.5[d]
$X23_{(TET)}$ tetramer	43	−50.8[c]	ND[h]	
$X23_{(TET)}$ monomer	ND[h]		55	−38.8[c]
Q165E-$X21_{(TCT)}$	77	5[e]	82	6[e]
S254K-$X21_{(TCT)}$	73	1[e]	75	−1[e]
Q165E/S254K-$X21_{(TCT)}$	77	5[e]	81	5[e]
D275P-$X23_{(TET)}$ tetramer	78	35[f]	ND[h]	
D275P-$X23_{(TET)}$ monomer	ND[h]		60	5[g]

[a] $T_{1/2}{}^{60\ min}$ is the temperature at which 50% of the enzymatic activity is lost after a 1 h incubation, interpolated from a plot of the residual enzymatic activity vs temperature. [b] $T_{1/2}{}^{CD}$ is the temperature at which 50% of the original CD signal at 218 nm is lost upon heating the protein sample between 30 and 98 °C (30 and 110 °C for TbADH), with an average increase in temperature at a rate of 1 °C/min. [c] Relative to TbADH. [d] Relative to CbADH. [e] Relative to $X21_{(TCT)}$. [f] Relative to $X23_{(TET)}$ tetramer. [g] Relative to $X23_{(TET)}$ monomer. [h] Nondetectable.

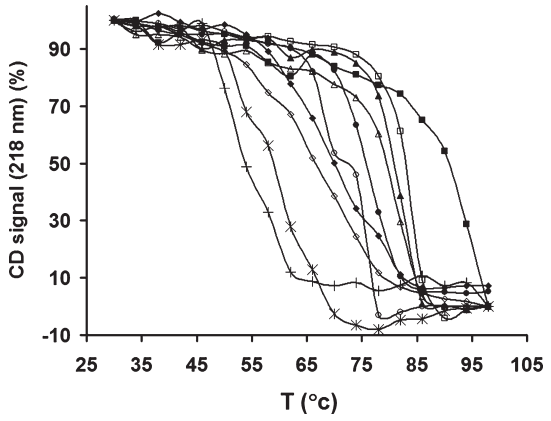

FIGURE 6: Effect of the mutations on the thermal stability of the secondary structure of the chimeric ADHs and their mutants. The thermal stability of the ADHs and their chimeric mutants was determined by monitoring the loss of their CD signal at 218 nm upon heating. The data (millidegrees vs wavelength) were collected every nanometer with an averaging time of 2 s using quartz cells with a light path of 0.1 cm. Experiments were performed between 30 and 98 °C, with an average increase in temperature of 1 °C/min. Scans were performed every 4 °C. The protein concentration was ~0.5 mg/mL in 50 mM Na/K phosphate buffer (pH 6.8). The background for each scan was determined in a single scan with buffer alone at 25 °C and subtracted from each scan. The background CD signal was temperature-independent: TbADH (■), EhADH1 (△), CbADH (◇), $X21_{(TCT)}$ (●), $X23_{(TET)}$ monomer (+), $X22_{(CTC)}$ (◆), S254K/Q165E-$X21_{(TCT)}$ (▲), S254K-$X21_{(TCT)}$ (○), Q165E-$X21_{(TCT)}$ (□), and D275P-$X23_{(TET)}$ monomer (∗).

No significant changes occurred in the Cα backbone of the chimeras (rmsd between 0.45 and 0.65 Å overall) compared with those of the parent enzymes, suggesting that the differences in the thermal stability of the chimeras and the parent enzymes could have originated from specific structural elements located at strategic points in the ADH molecules.

Site-Directed Mutagenesis (SDM) of Chimeric ADHs. (*i*) *Mutagenesis of an Ion Pair and of the Intersubunit Ion Pair Network of* $X21_{(TCT)}$. In both TbADH and CbADH, Lys257 and Asp237 form an intrasubunit ion pair (*20*),

Table 3: Crystallographic Data Collection and Refinement Statistics

	$X23_{(TET)}$	$X22_{(CTC)}$	$X21_{(TCT)}$	Q165E/S254K-$X21_{(TCT)}$
Crystal Data				
source	ESRF	ESRF	Rigaku RUH3R	Rigaku RUH3R
temperature (K)	100	100	110	110
space group	$P2_1$	$I23$	$P2_1$	$P2_1$
unit cell parameters	a = 79.75 Å b = 82.44 Å c = 118.26 Å β = 99.89°	$a = b = c$ = 129.48 Å	a = 79.29 Å b = 101.43 Å c = 113.17 Å β = 94.2°	a = 79.34 Å b = 83.00 Å c = 119.69 Å β = 99.93°
Internal Scaling				
resolution (Å)	116.25−1.40 (1.42−1.40)	91.67−1.90 (1.95−1.90)	50−2.2 (2.24−2.20)	50−2.2 (2.24−2.20)
no. of reflections measured	906187 (31523)	324180 (23647)	225662 (11240)	242801 (12250)
no. of unique reflections	278316 (13706)	27015 (2004)	90320 (4499)	76750 (3820)
completeness (%)	99.3 (98.3)	99.7 (99.8)	99.7 (100.0)	97.8 (99.1)
R_{merge}[a]	0.074 (0.58)	0.068 (0.44)	0.071 (0.53)	0.092 (0.35)
$I/\sigma(I)$ (average)	28.2 (1.4)	30.2 (2.2)	11.40 (2.1)	11.60 (3.02)
Model Refinement				
resolution range (Å)	116.25−1.40 (1.44−1.40)	91.67−1.90 (1.95−1.90)	110.80−2.20 (2.26−2.20)	50−2.2 (2.24−2.20)
no. of molecules per asymmetric unit	4	1	4	4
no. of protein residues	1404	351	1404	1404
Wilson B factor (Å^2)	11.23	17.40	28.80	38.20
overall B factor (Å^2)	9.92	17.90	41.64	47.10
R_{cryst}	0.140 (0.250)	0.125 (0.167)	0.174 (0.263)	0.169 (0.195)
R_{free} (5% of data)	0.165 (0.263)	0.172 (0.228)	0.225 (0.329)	0.223 (0.296)
Geometry				
rmsd for bonds (Å)	0.014	0.016	0.014	0.012
rmsd for bond angles (Å)	1.534	1.553	1.523	0.0135
rmsd for planar groups (Å)	0.007	0.006	0.005	0.004
estimated coordinate error (Å)	0.032	0.072	0.143	0.161
Ramachandran Statistics				
% (residues) for non-Gly and non-Pro residues				
most favored	89.5 (1031)	90.0 (262)	88.6 (1014)	88.4 (1011)
additional allowed	10.5 (121)	10.0 (29)	11.3 (129)	11.4 (130)
disallowed regions	0.0 (0)	0.0 (0)	0.1 (1)	0.1 (1)

[a] $R_{merge} = |I_i(hkl) - \langle I(hkl)\rangle|/I_i(hkl)$, where (hkl) denotes the sum over all reflections and i the sum over all equivalent and symmetry-related reflections (*53*). Values in parentheses are for the highest resolution shell.

yet in TbADH, Asp237 is also involved in an ion pair bridge with Arg304 of a second subunit. Arg304, in turn, forms an additional intersubunit salt bridge with Glu165 of the first subunit. Thus, in TbADH, a four-member ion pair network involving $Lys257^A$, $Asp237^A$, $Arg304^D$, and $Glu165^A$ is present (the superscript refers to the subunit). All four side chain functional groups are located on the surface of the respective subunits (*20*). In the mesophilic CbADH, such an ion pair network does not exist, since both Arg304 and Glu165 are replaced with Met304 and Gln165, respectively, whose side chains do not interact electrostatically (*20*). Indeed, reconstruction of this network by SDM has led to significant enhancement of the thermal stability of CbADH ($\Delta T_{1/2}^{60\ min}$ = 5.4 °C) (*20*).

The respective residues 165 of $X21_{(TCT)}$ and 304 of $X22_{(CTC)}$ originate from CbADH; hence, the network described above is incomplete in both chimeras.

Likewise, the replacement of Ser254 of CbADH with Lys significantly enhances the stability of the enzyme, due to the formation of intrasubunit Lys254 and Glu280 ion pair (*20*). In $X21_{(TCT)}$, position 254 is occupied by Ser (CbADH). Inspection of the 3D structures of $X21_{(TCT)}$ showed that the $Lys257^A$-$Asp237^A$-$Arg304^D$-$Glu165^A$ intersubunit ion pair network, as well as the Lys254-Glu280 ion pair, could be reconstructed in $X21_{(TCT)}$. Therefore, in an attempt to enhance the thermal stability of $X21_{(TCT)}$, we substituted both Gln165 and Ser254 of $X21_{(TCT)}$ with Glu and Lys, respectively, both independently and in combination, thereby forming mutant chimeras Q165E-$X21_{(TCT)}$, S254K-$X21_{(TCT)}$, and Q165E/S254K-$X21_{(TCT)}$.

The thermal stability parameters of this mutant chimera, determined as described above, are presented in Table 2. The thermal stability of Q165E-$X21_{(TCT)}$ was significantly enhanced over that of $X21_{(TCT)}$ ($\Delta T_{1/2}^{60\ min}$ = 5 °C, and $\Delta T_{1/2}^{CD}$ = 6 °C), suggesting that the intersubunit ion pair network was reconstructed and stabilized the $X21_{(TCT)}$ chimera. Replacing Ser254 with Lys had a negligible effect on the $T_{1/2}^{60\ min}$ and $T_{1/2}^{CD}$ values of $X21_{(TCT)}$ (1 and −1 °C, respectively). The thermal stability of Q165E/S254K-$X21_{(TCT)}$ was not higher than that of the single mutant Q165E-$X21_{(TCT)}$ ($\Delta T_{1/2}^{60\ min}$ = 5 °C, and $\Delta T_{1/2}^{CD}$ = 5 °C).

(*ii*) *3D Structure of Q165E/S254K-X21$_{(TCT)}$*. The 3D structure of Q165E/S254K-$X21_{(TCT)}$ was determined by X-ray crystallography to a resolution of 2.2 Å. Analysis of the structure indicated that the $Lys257^A$-$Asp237^A$-$Arg304^D$-$Glu165^A$ intersubunit ion pair network was indeed reconstructed in the mutant chimera, as presented in Figure 7. Further inspection of the

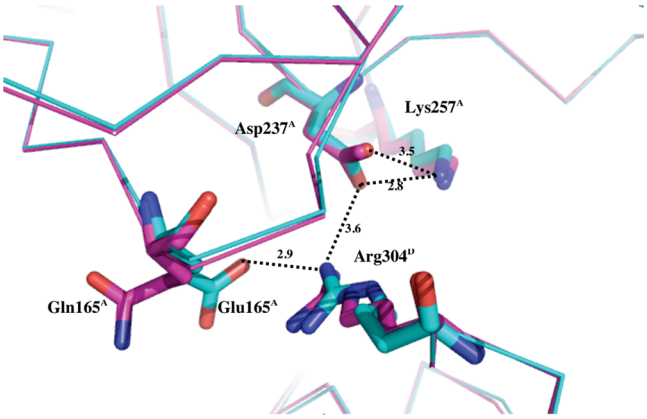

FIGURE 7: Intersubunit K257^{A}-D237^{A}-R304^{D}-E165^{A} ion network of Q165E/S254K-X21$_{(TCT)}$ (the superscript refers to the subunit). The ion pairs are depicted in dashes and the lengths in angstroms. The backbone and residues of parent chimera X21$_{(TCT)}$ are colored magenta and those of the double mutant Q165E/S254K-X21$_{(TCT)}$ cyan.

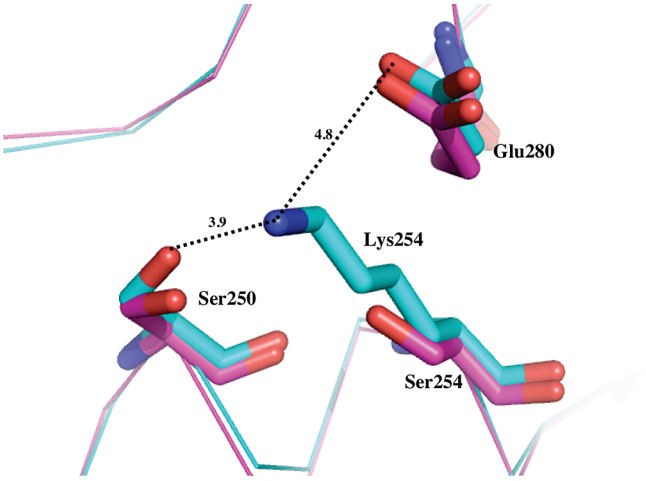

FIGURE 8: Intrasubunit K254-E280 ion pair and K254−S250 charged neutral hydrogen bond of Q165E/S254K-X21$_{(TCT)}$. The ion pairs and the hydrogen bond are depicted as dashes and the lengths in angstroms. The backbone and residues of parent chimera X21$_{(TCT)}$ are colored magenta and those of the double mutant Q165E/S254K-X21$_{(TCT)}$ cyan.

double mutant structure revealed that Lys254 is involved in a long-range intrasubunit ion pair with Glu280 and, by a charged neutral hydrogen bond, with Ser250, as demonstrated in Figure 8.

(*iii*) *SDM at the Dimerization Interface of* X23$_{(TET)}$. Pro275 of TbADH, located in the middle of the horse liver ADH-type dimer of TbADH, plays a significant role in maintaining the thermal stability of the ADH (*19*). Similar to its parent EhADH1, chimera X23$_{(TET)}$ contains Asp at position 275. As we found that substituting Asp for Pro at that position stabilizes EhADH1 (*41*), we wondered whether this mutation would also stabilize X23$_{(TET)}$ and produced mutant D275P-X23$_{(TET)}$.

(*iv*) *Quaternary Structure of D275P-*X23$_{(TET)}$. Unlike its parent chimera X23$_{(TET)}$, the purified D275P-X23$_{(TET)}$ mutant was found to be a tetramer in solution [on Superdex 200 size exclusion chromatography (Figure 3)] and showed an enzymatic activity comparable to that of the parent ADHs (data not shown). These findings suggested that via introduction of proline at position 275, the oligomeric integrity of chimera D275P-X23$_{(TET)}$ would be maintained, probably because of an increase in the rigidity of the dimerization interface (*17*). Nevertheless, the tetrameric chimeric mutant constructed here was less stable than the tetrameric parent ADHs (TbADH and EhADH1). Upon 2-fold dilution and dialysis for 16 h against phosphate buffer at 4 °C, the chromatographic peak of tetrameric D275P-X23$_{(TET)}$ broadened, suggesting its aggregation to a higher-molecular mass species; the fraction of monomeric D275P-X23$_{(TET)}$ was significantly increased (data not shown).

This finding suggested that additional stabilizing structural motifs of the parent ADHs are absent from both X23$_{(TET)}$ and D275P-X23$_{(TET)}$.

*Thermal Stability Parameters of D275P-*X23$_{(TET)}$. The thermal stability parameters of the mutant chimera, determined as described above, are presented in Table 2. The thermal stability of enzymatically active tetrameric D275P-X23$_{(TET)}$ was significantly higher than that of tetrameric X23$_{(TET)}$ ($\Delta T_{1/2}^{60\ min}$ = 35 °C). We therefore assume that this mutation maintains the integrity of the tetramer, hence stabilizing the enzyme against thermal inactivation.

The thermal stability of the monomeric species of both X23$_{(TET)}$ and D275P-X23$_{(TET)}$ was studied using CD spectroscopy. The $T_{1/2}^{CD}$ value of the monomeric mutant chimera was significantly higher than that of its monomeric parent chimera [$\Delta T_{1/2}^{CD}$ = 5 °C (Table 2)]. We propose that the contribution of Pro275 to the thermal stability of this chimera mutant is not caused solely by the maintenance of the quaternary structure of the protein molecule but is also manifested at the level of the polypeptide chain.

DISCUSSION

Molecular chimeras engineered from homologous proteins have been widely used to assess the contribution of specific domains to the stability of the protein molecule (*1*). We applied this approach to examine the contribution of the structurally distinct cofactor-binding domain (residues 153−295) and the catalytic domain (residues 1−152 and 296−351/2) of TbADH (T), CbADH (C), and EhADH1 (E) to their thermostability.

In the first chimera, X21$_{(TCT)}$, the cofactor-binding domain of TbADH was replaced with the cofactor-binding domain of CbADH. This domain exchange significantly destabilized the parent thermophilic TbADH ($\Delta T_{1/2}^{60\ min}$ = −22 °C, and $\Delta T_{1/2}^{CD}$ = −18 °C). The reverse exchange in CbADH, chimera X22$_{(CTC)}$, however, had little effect on the thermal stability of the parent CbADH ($\Delta T_{1/2}^{60\ min}$ = −0.5 °C, and $\Delta T_{1/2}^{CD}$ = 2.5 °C).

The enzymatic activities of the parent ADHs were preserved in both chimeras. This profound difference in the outcome of the domain switching could have originated from an imperfect fit of the "guest" domain in the "host" molecule. Because the overall 3D structures of the Cα backbones of the chimeras are superposable with those of the parent enzymes (see, e.g., Figure 9), however, the impact of the domain switch on the thermal stability of the resulting chimeras might result from interferance with specific stabilizing elements that involve interdomain associations. In a similar study, Sanderova et al. (*42*) suggested that the thermostability of elongation factor Tu (EF-Tu) chimeras, composed of domains derived from the mesophilic *Es. coli* EF-Tu and the thermophilic *Bacillus stearothermophilus* EF-Tu, could be the result of cooperative interactions between the domains.

The third chimera X23$_{(TET)}$, in which the cofactor-binding domain of EhADH1 replaced the cofactor-binding domain of TbADH, disintegrated readily into monomers. CD spectroscopy

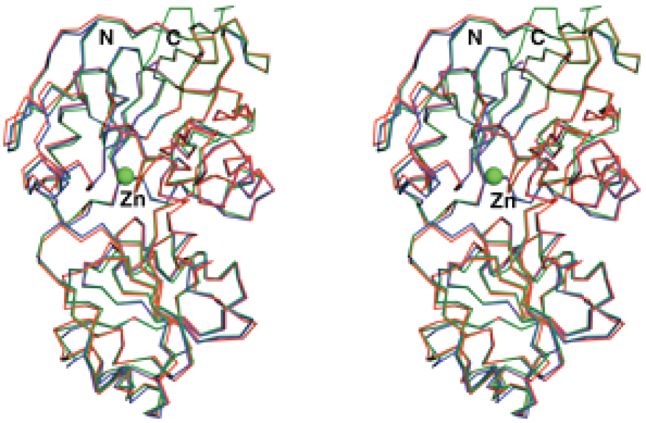

FIGURE 9: Typical Cα trace superposition for the $X23_{(TET)}$ chimera and its parent ADHs represented in stereo. Structures of TbADH (red), EhADH1 (green), and chimera $X23_{(TET)}$ (blue) are superimposed. The catalytic and coenzyme-binding domains are shown in the top and bottom parts of the picture, respectively. The rmsd's of the TbADH−EhADH1, TbADH−$X23_{(TET)}$, and EhADH1−$X23_{(TET)}$ superimposed pairs are 0.68, 0.56, and 0.48 Å, respectively.

measurements indicated that the secondary structure of the $X23_{(TET)}$ monomer was indistinguishable from the CD spectra of its tetrameric ADH parents and showed a sharp CD signal drop as a function of temperature, an indication of a well-defined structure. The finding that this chimera was enzymatically inactive indicates that the structural integrity of the tetramer is prerequisite for the expression of enzymatic activity in these ADHs. At high protein concentrations, however, the $X23_{(TET)}$ monomers associated into enzymatically active tetramers that could be crystallized as a tetrameric chimera, with no crystals of monomeric $X23_{(TET)}$ being found.

Olofsson studied the enzymatic activity of TbADH in solutions of aqueous organic solvents and suggested (*43*) that the tetrameric form of TbADH is not critical for its catalytic activity, yet in that study, no direct evidence was presented showing the actual presence of enzymatically active monomeric or dimeric species. In our study, the enzymatic activity of $X23_{(TET)}$, a TbADH chimeric mutant, was monitored after a prolonged incubation of the enzyme with substrate. Under such conditions, trace amounts of the tetramer could have been easily formed to catalyze the reaction. Our findings showing the presence of tetrameric species in the largely monomeric solutions of $X23_{(TET)}$, especially after prolonged incubation, provide evidence for equilibrium among the different oligomeric species.

The finding that chimera $X23_{(TET)}$ was relatively unstable compared with its parent ADHs ($\Delta T_{1/2}^{60\ min} \leq 51$ °C, and $\Delta T_{1/2}^{CD} \leq 39$ °C) indicates that the integrity of the tetramer is a major factor in maintaining the thermal stability of the tetrameric ADHs. The similarity of the overall 3D structures of the thermophilic TbADH and the chimera $X23_{(TET)}$ together with the absence of a significant deviation in the Cα backbone of the chimera and its parent enzyme led us to postulate that the thermal stability of $X23_{(TET)}$ could be enhanced through specific substitutions at structurally strategic positions.

The findings of this study support the observations of Kumar and Nussinov, who compared the organization of salt bridges and ion pair networks in homologous citrate synthases from the hyperthermophile *Pyrococcus furiosus*, from chicken, and from the psychrophile (cold adapted) *Arthobacter* Ds2-3R (*44*). The authors showed that unlike the mesophilic and psychrophilic enzymes, salt bridges and their networks in the thermophilic enzyme largely cluster in the active site regions and at the dimer interface, thus contributing to the integrity of both the protein dimer and the active site by possibly countering conformational disorder at high temperatures. On the other hand, in the psychrophilic enzyme at low temperatures, electrostatics may contribute to the enhancement of protein solvation and ensure active site flexibility (*44*).

In the thermophilic TbADH studied here, the extensive $Lys257^{A}$-$Asp237^{A}$-$Arg304^{D}$-$Glu165^{A}$ intersubunit ion pair network [superscript denotes the subunit (*19*)] involves residues on the surface of both domains. Although a domain change in chimera $X21_{(TCT)}$ interrupted this network, the site-directed mutation Q165E-$X21_{(TCT)}$ concomitantly reconstructed the intersubunit ion pair part of the network and enhanced the thermal stability of the chimera ($\Delta T_{1/2}^{60\ min} = 5$ °C, and $\Delta T_{1/2}^{CD} = 6$ °C).

The stabilization of proteins via a reduction in the entropy of the unfolded state through the introduction of proline residues is well-documented (*19*, *45*−*47*). Proline seems to be an ideal candidate for thermostabilizing proteins because its pyrrolidine ring adopts fewer conformations than does any other amino acid. Suzuki (*48*) analyzed the critical sites for protein thermostabilization by proline. According to the "Suzuki rule", a protein can be stabilized when prolines are inserted at certain strategic positions, namely, the second site of the β turn or the N-cap of the α helix and flexible loops.

The most effective stabilization of a chimeric ADH was demonstrated with chimera $X23_{(TET)}$. Replacing Asp275 with proline induced the oligomerization of chimeric mutant D275P-$X23_{(TET)}$ into homotetramers at a relatively low protein concentration (micrograms per milliliter). Oligomerization could be achieved in the parent chimera $X23_{(TET)}$ only at very high protein concentrations (during crystallization trials at concentrations of 8−10 mg/mL). Site-directed mutation of a single codon of an amino acid, located in the center of the dimerization interface between two monomers, was sufficient to induce such a major transformation. The remarkable thermal stability of this mutant ($\Delta T_{1/2}^{60\ min} = 35$ °C) indicates a strong dependence of the thermal stability of the ADH on its quaternary structure, which can be manipulated by a minimal number of mutations.

Outline of the Crystallographic Results. The structures of the chimeric ADHs described in this study have been deposited in the Protein Data Bank [entry 3FSR for chimera $X21_{(TCT)}$, entry 3FPL for $X22_{(CTC)}$, entry 3FPC for $X23_{(TET)}$, and entry 3FTN for Q165E/S254K-$X21_{(TCT)}$], as were the previously determined structures of their parent ADHs (entry 1PED for TbADH, entry 1KEV for CbADH, and entry 1Y9A for EhADH1).

Analysis of the structure of Q165E/S254K-$X21_{(TCT)}$ indicated that the $Lys257^{A}$-$Asp237^{A}$-$Arg304^{D}$-$Glu165^{A}$ intersubunit ion network was reconstructed in the mutant chimera, as presented in Figure 7. Further inspection of the mutant structure revealed that Lys254 is involved in a long-range intrasubunit ion pair with Glu280 and, by a charged neutral hydrogen bond, with Ser250, as demonstrated in Figure 8.

It was previously suggested that salt bridge networks that are energetically more favorable than isolated ion pairs (*49*) are the most prominent structural features that can explain the unusual properties of certain extreme thermophiles and hyperthermophiles (*50*−*52*). Our results support this observation since the reconstruction of the intersubunit ion pair network increased the thermostability of the $X21_{(TCT)}$ chimera more than the intrasubunit long-range ion pair and the charged neutral hydrogen bond.

ACKNOWLEDGMENT

We acknowledge the ESRF (Grenoble, France) for the use of the macromolecular crystallographic data collection facilities and the ID14eh cluster staff for their assistance. We thank Dr. Harry Greenblatt for collecting X-ray data with our home diffractometer and Dr. Virginia Buchner for helpful discussions during manuscript preparation.

REFERENCES

1. Luong, T. N., and Kirsch, J. F. (2001) A general method for the quantitative analysis of functional chimeras: Applications from site-directed mutagenesis and macromolecular association. *Protein Sci. 10*, 581–591.
2. Wells, J. A. (1990) Additivity of mutational effects in proteins. *Biochemistry 29*, 8509–8517.
3. Li, Y., Drummond, D. A., Sawayama, A. M., Snow, C. D., Bloom, J. D., and Arnold, F. H. (2007) A diverse family of thermostable cytochrome P450s created by recombination of stabilizing fragments. *Nat. Biotechnol. 25*, 1051–1056.
4. Heinzelman, P., Snow, C. D., Wu, I., Nguyen, C., Villalobos, A., Govindarajan, S., Minshull, J., and Arnold, F. H. (2009) A family of thermostable fungal cellulases created by structure-guided recombination. *Proc. Natl. Acad. Sci. U.S.A. 106*, 5610–5615.
5. Bergeron, L. M., Gomez, L., Whitehead, T. A., and Clark, D. S. (2009) Self-renaturing enzymes: Design of an enzyme-chaperone chimera as a new approach to enzyme stabilization. *Biotechnol. Bioeng. 102*, 1316–1322.
6. Asada, Y., Endo, S., Inoue, Y., Mamiya, H., Hara, A., Kunishima, N., and Matsunaga, T. (2009) Biochemical and structural characterization of a short-chain dehydrogenase/reductase of *Thermus thermophilus* HB8: A hyperthermostable aldose-1-dehydrogenase with broad substrate specificity. *Chem.-Biol. Interact. 178*, 117–126.
7. Loveridge, E. J., Rodriguez, R. J., Swanwick, R. S., and Allemann, R. K. (2009) Effect of dimerization on the stability and catalytic activity of dihydrofolate reductase from the hyperthermophile *Thermotoga maritima*. *Biochemistry 48*, 5922–5933.
8. Asako, H., Shimizu, M., and Itoh, N. (2008) Engineering of NADPH-dependent aldo-keto reductase from *Penicillium citrinum* by directed evolution to improve thermostability and enantioselectivity. *Appl. Microbiol. Biotechnol. 80*, 805–812.
9. Bolivar, J. M., Cava, F., Mateo, C., Rocha-Martín, J., Guisán, J. M., Berenguer, J., and Fernandez-Lafuente, R. (2008) Immobilization-stabilization of a new recombinant glutamate dehydrogenase from *Thermus thermophilus*. *Appl. Microbiol. Biotechnol. 80*, 49–58.
10. Levin, I., Meiri, G., Peretz, M., Burstein, Y., and Frolow, F. (2004) The ternary complex of *Pseudomonas aeruginosa* alcohol dehydrogenase with NADH and ethylene glycol. *Protein Sci. 13*, 1547–1556.
11. Peretz, M., and Burstein, Y. (1989) Amino acid sequence of alcohol dehydrogenase from the thermophilic bacterium *Thermoanaerobium brockii*. *Biochemistry 28*, 6549–6555.
12. Burdette, D. S., Tchernajencko, V. V., and Zeikus, J. G. (2000) Effect of thermal and chemical denaturants on *Thermoanaerobacter ethanolicus* secondary-alcohol dehydrogenase stability and activity. *Enzyme Microb. Technol. 27*, 11–18.
13. Musa, M. M., Ziegelmann-Fjeld, K. I., Vieille, C., Zeikus, J. G., and Phillips, R. S. (2007) Asymmetric reduction and oxidation of aromatic ketones and alcohols using W110A secondary alcohol dehydrogenase from *Thermoanaerobacter ethanolicus*. *J. Org. Chem. 72*, 30–34.
14. Musa, M. M., Ziegelmann-Fjeld, K. I., Vieille, C., and Phillips, R. S. (2008) Activity and selectivity of W110A secondary alcohol dehydrogenase from *Thermoanaerobacter ethanolicus* in organic solvents and ionic liquids: Mono- and biphasic media. *Org. Biomol. Chem. 6*, 887–892.
15. Kumar, A., Shen, P. S., Descoteaux, S., Pohl, J., Bailey, G., and Samuelson, J. (1992) Cloning and expression of an $NADP^+$-dependent alcohol dehydrogenase gene of *Entamoeba histolytica*. *Proc. Natl. Acad. Sci. U.S.A. 89*, 10188–10192.
16. Peretz, M., Bogin, O., Tel-Or, S., Cohen, A., Li, G., Chen, J. S., and Burstein, Y. (1997) Molecular cloning, nucleotide sequencing, and expression of genes encoding alcohol dehydrogenases from the thermophile *Thermoanaerobacter brockii* and the mesophile *Clostridium beijerinckii*. *Anaerobe 3*, 259–270.
17. Korkhin, Y., Kalb (Gilboa), A. J., Peretz, M., Bogin, O., Burstein, Y., and Frolow, F. (1999) Oligomeric integrity: The structural key to thermal stability in bacterial alcohol dehydrogenases. *Protein Sci. 8*, 1241–1249.
18. Shimon, L. J., Goihberg, E., Peretz, M., Burstein, Y., and Frolow, F. (2006) Structure of alcohol dehydrogenase from *Entamoeba histolytica*. *Acta Crystallogr. D62*, 541–547.
19. Bogin, O., Peretz, M., Hacham, Y., Korkhin, Y., Frolow, F., Kalb (Gilboa), A. J., and Burstein, Y. (1998) Enhanced thermal stability of *Clostridium beijerinckii* alcohol dehydrogenase after strategic substitution of amino acid residues with prolines from the homologous thermophilic *Thermoanaerobacter brockii* alcohol dehydrogenase. *Protein Sci. 7*, 1156–1163.
20. Bogin, O., Levin, I., Hacham, Y., Tel-Or, S., Peretz, M., Frolow, F., and Burstein, Y. (2002) Structural basis for the enhanced thermal stability of alcohol dehydrogenase mutants from the mesophilic bacterium *Clostridium beijerinckii*: Contribution of salt bridging. *Protein Sci. 11*, 2561–2574.
21. Bogin, O., Peretz, M., and Burstein, Y. (1998) Probing structural elements of thermal stability in bacterial oligomeric alcohol dehydrogenases. I. Construction and characterization of chimeras consisting of secondary ADHs from *Thermoanaerobacter brockii* and *Clostridium beijerinckii*. *Lett. Pept. Sci. 5*, 399–408.
22. Goihberg, E., Dym, O., Tel-Or, S., Shimon, L., Frolow, F., Peretz, M., and Burstein, Y. (2008) Thermal stabilization of the protozoan *Entamoeba histolytica* alcohol dehydrogenase by a single proline substitution. *Proteins 72*, 711–719.
23. Bogin, O., Yayon, A., Peretz, M., and Burstein, Y. (2000) High level expression of heterologous proteins. Israel Patent 138529; U.S. and Int. Patent PCT/IL01/00870.
24. Bradford, M. M. (1976) A rapid and sensitive method for the quantitation of microgram quantities of protein utilizing the principle of protein-dye binding. *Anal. Biochem. 72*, 248–254.
25. Sanger, F., and Coulson, A. R. (1975) A rapid method for determining sequences in DNA by primed synthesis with DNA polymerase. *J. Mol. Biol. 94*, 441–448.
26. Laemmli, U. K. (1970) Cleavage of structural proteins during the assembly of the head of bacteriophage T4. *Nature 227*, 680–685.
27. Teng, T. Y. (1990) Mounting of Crystals for Macromolecular Crystallography in a Freestanding Thin-Film. *J. Appl. Crystallogr. 23*, 387–391.
28. Otwinowski, Z., and Minor, W. (1997) Processing of X-ray diffraction data collected in oscillation mode. *Methods Enzymol. 276*, 307–326.
29. Vagin, A., and Teplyakov, A. (1997) MOLREP: An automated program for molecular replacement. *J. Appl. Crystallogr. 30*, 1022–1025.
30. Murshudov, G. N., Vagin, A. A., and Dodson, E. J. (1997) Refinement of macromolecular structures by the maximum-likelihood method. *Acta Crystallogr. D53*, 240–255.
31. Bailey, S. (1994) The CCP4 Suite: Programs for Protein Crystallography. *Acta Crystallogr. D50*, 760–763.
32. Potterton, E., Briggs, P., Turkenburg, M., and Dodson, E. (2003) A graphical user interface to the CCP4 program suite. *Acta Crystallogr. D59*, 1131–1137.
33. Brunger, A. T. (1992) Free R value: A novel statistical quantity for assessing the accuracy of crystal structures. *Nature 355*, 472–475.
34. Perrakis, A., Morris, R., and Lamzin, V. S. (1999) Automated protein model building combined with iterative structure refinement. *Nat. Struct. Biol. 6*, 458–463.
35. Emsley, P., and Cowtan, K. (2004) Coot: Model-building tools for molecular graphics. *Acta Crystallogr. D60*, 2126–2132.
36. Winn, M. D., Murshudov, G. N., and Papiz, M. Z. (2003) Macromolecular TLS refinement in REFMAC at moderate resolutions. *Methods Enzymol. 374*, 300–321.
37. Laskowski, R. A., Macarthur, M. W., Moss, D. S., and Thornton, J. M. (1993) Procheck: A Program to Check the Stereochemical Quality of Protein Structures. *J. Appl. Crystallogr. 26*, 283–291.
38. Vriend, G. (1990) What If: A Molecular Modeling and Drug Design Program. *J. Mol. Graphics 8*, 52–56.
39. Davis, I. W., Leaver-Fay, A., Chen, V. B., Block, J. N., Kapral, G. J., Wang, X., Murray, L. W., Arendall, W. B., III, Snoeyink, J., Richardson, J. S., and Richardson, D. C. (2007) MolProbity: All-atom contacts and structure validation for proteins and nucleic acids. *Nucleic Acids Res. 35*, W375–W383.
40. Hawe, A., Sutter, M., and Jiskoot, W. (2008) Extrinsic fluorescent dyes as tools for protein characterization. *Pharm. Res. 25*, 1487–1499.
41. Goihberg, E., Dym, O., Tel-Or, S., Levin, I., Peretz, M., and Burstein, Y. (2007) A single proline substitution is critical for the thermostabilization of *Clostridium beijerinckii* alcohol dehydrogenase. *Proteins 66*, 196–204.
42. Sanderova, H., Hulkova, M., Malon, P., Kepkova, M., and Jonak, J. (2004) Thermostability of multidomain proteins: Elongation factors EF-Tu from *Escherichia coli* and *Bacillus stearothermophilus* and their chimeric forms. *Protein Sci. 13*, 89–99.

43. Olofsson, L., Nicholls, I. A., and Wikman, S. (2005) TBADH activity in water-miscible organic solvents: Correlations between enzyme performance, enantioselectivity and protein structure through spectroscopic studies. *Org. Biomol. Chem. 3*, 750–755.
44. Kumar, S., and Nussinov, R. (2004) Different roles of electrostatics in heat and in cold: Adaptation by citrate synthase. *ChemBioChem 5*, 280–290.
45. Matthews, B. W., Nicholson, H., and Becktel, W. J. (1987) Enhanced protein thermostability from site-directed mutations that decrease the entropy of unfolding. *Proc. Natl. Acad. Sci. U.S.A. 84*, 6663–6667.
46. Sriprapundh, D., Vieille, C., and Zeikus, J. G. (2000) Molecular determinants of xylose isomerase thermal stability and activity: Analysis of thermozymes by site-directed mutagenesis. *Protein Eng. 13*, 259–265.
47. Marciano, D. C., Pennington, J. M., Wang, X., Wang, J., Chen, Y., Thomas, V. L., Shoichet, B. K., and Palzkill, T. (2008) Genetic and structural characterization of an L201P global suppressor substitution in TEM-1β-lactamase. *J. Mol. Biol. 384*, 151–164.
48. Watanabe, K., Masuda, T., Ohashi, H., Mihara, H., and Suzuki, Y. (1994) Multiple proline substitutions cumulatively thermostabilize *Bacillus cereus* ATCC7064 oligo-1,6-glucosidase. Irrefragable proof supporting the proline rule. *Eur. J. Biochem. 226*, 277–283.
49. Horovitz, A., Serrano, L., Avron, B., Bycroft, M., and Fersht, A. R. (1990) Strength and co-operativity of contributions of surface salt bridges to protein stability. *J. Mol. Biol. 216*, 1031–1044.
50. Yip, K. S., Stillman, T. J., Britton, K. L., Artymiuk, P. J., Baker, P. J., Sedelnikova, S. E., Engel, P. C., Pasquo, A., Chiaraluce, R., and Consalvi, V. (1995) The structure of *Pyrococcus furiosus* glutamate dehydrogenase reveals a key role for ion-pair networks in maintaining enzyme stability at extreme temperatures. *Structure 3*, 1147–1158.
51. Hennig, M., Sterner, R., Kirschner, K., and Jansonius, J. N. (1997) Crystal structure at 2.0 Å resolution of phosphoribosyl anthranilate isomerase from the hyperthermophile *Thermotoga maritima*: Possible determinants of protein stability. *Biochemistry 36*, 6009–6016.
52. Pappenberger, G., Schurig, H., and Jaenicke, R. (1997) Disruption of an ionic network leads to accelerated thermal denaturation of D-glyceraldehyde-3-phosphate dehydrogenase from the hyperthermophilic bacterium *Thermotoga maritima*. *J. Mol. Biol. 274*, 676–683.
53. Stout, G. H., and Jensen, L. H. (1968) X-ray Structure Determination. A Practical Guide, MacMillan, London.